Probing metal complex dissociation in cells by fluorescence microscopy

Contact *s.w.botchway@ral.ac.uk*

J. R. Dilworth, S. Faulkner, M. W. Jones, M. B. M. Theobald and P. A. Waghorn

University of Oxford
Inorganic Chemistry Laboratory, South Parks Road, Oxford

S. I. Pascu and R. L. Arrowsmith

University of Bath, Chemistry Department, Claverton Down, Bath, Avon, BA2 7AY

S. W. Botchway and A. W. Parker

CLF
RAL, Harwell, Oxon

Introduction

SPECT and PET agents based on gamma or positron metallic radionuclides are in widespread use for the diagnosis of a number of diseases whilst beta or auger electron emitting radionuclides are used for therapy. Some important classes of imaging agent depend on intracellular processes to achieve selectivity, however the resolution limit for nuclear medicine of 1-2mm means that little is known about their speciation within living cells. Confocal fluorescence microscopy has been used extensively to track compounds and follow processes in cells. Subsequently we have designed a series of fluorescent metal complexes which can be used for whole body imaging using gamma or positron emission and followed in cells by virtue of their 1 or 2-photon fluorescence. We are particularly interested in the complexes of metallic radionuclides where a key step in their biological action can be dissociation of the complex within cells. The emission lifetime and emission wavelength of a ligand changes when a metal is coordinated and this provides a potential method to determine when and where dissociation of a metal complex occurs within a cell. We have explored the use of this approach to determine if and when intracellular demetallation of biologically active metal complexes occurs. The chemical series of current interest, design and research within this collaboration is; copper bis(thiosemicarbazone) complexes, indium tridentate thiosemicarbazones and indium porphyrins.

Copper bis(thiosemicarbazone) complexes

Bis(thiosemicarbazone) complexes of 64-copper(II) such as CuATSM (Figure 1) are in current clinical use for the imaging of hypoxia[1] although their performance is far from ideal. The hypoxia selectivity depends on the reduction of the complexes in hypoxic cells followed by dissociation and trapping of the copper. However, very little is known about the dissociative process and as the simple CuATSM complex is not fluorescent we have attached potent fluorophores (i.e. bodipy, fluorescein and anthracene) to the CuATSM core in order to follow the fate of the complexes in cells, Figure 2.

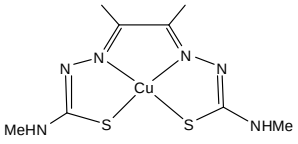

***Figure 1**: CuATSM*

The fluorescence emission data for the anthracene conjugates show that the free ligand and Cu complex emit at very distinct wavelengths, 510 nm and 450 nm respectively, which means that it should be possible to distinguish them in cells by the spectral analysis of the emitted fluorescence. The emission lifetime data for the bodipy and fluorescein conjugates suggest that it is, in principle, possible to discriminate between free ligand and copper complexes in cells. In the case of the bodipy adducts a change in lifetime from 4.1 ns for the free ligand to a lifetime of 2.9 ns for the copper complex is observed, which allows a level of discrimination between the two species *in vitro.*

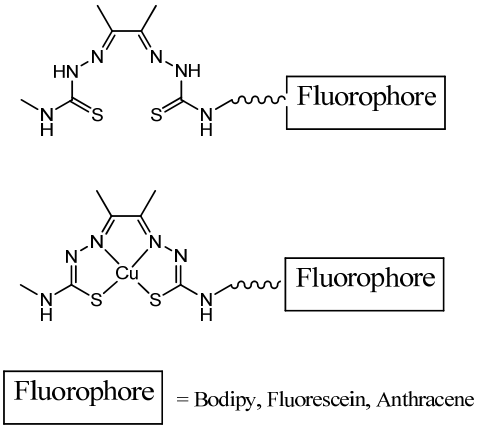

***Figure 2**: Structures of fluorescent CuATSM adducts*

Figure 3 shows lifetime emission maps for the free bodipy/ATSM ligand and the Cu complex in HeLa cells after 1 h incubation with the data suggesting that the Cu complex does not dissociate over time. This experiment was conducted under normoxic conditions so the lack of dissociation *via* reduction is not unexpected. We are currently investigating the hypoxia selectivity of the conjugate *via* 64-copper radiolabelling and will conduct the cell experiments under hypoxic conditions to establish quantification of the degree of dissociation.

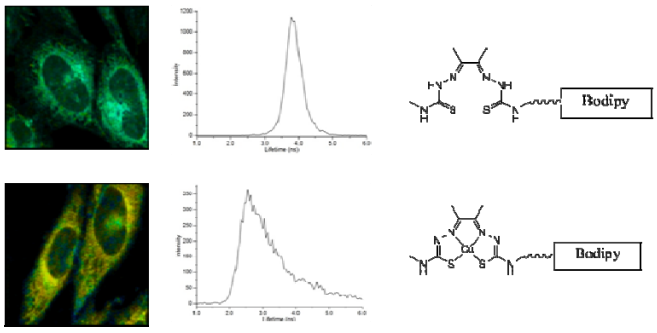

***Figure 3**: Emission lifetime maps for free bodipy/ATSM ligand(1) (top) and copper complex(3) (bottom).*

Furthermore, new Group 11, 12 and 13 metallic bis(thiosemicarbazonato) complexes with extremely highly kinetic stabilities in serum have also been investigated as potential alternative synthetic platforms for the simultaneous diagnosis and therapy of cancer.[2,3] This new family of intrinsically fluorescent metal bis(thiosemicarbazones) is shown in Figure 4 below, where M = Zn(II), Cu (II), Ga(III)Cl, In(III) and R = Me, Et, Ph and Allyl. Two photon spectroscopy (λ_{ex} 910 nm) was recorded in a variety of solvents and concentrations on the ligands and corresponding complexes. These complexes showed potent cytotoxicity in a number of

cell lines, coupled with interesting coordination modes for the ligand i.e. a symmetric and asymmetric mode, as shown by X-ray diffraction for M=Zn(II). [2]

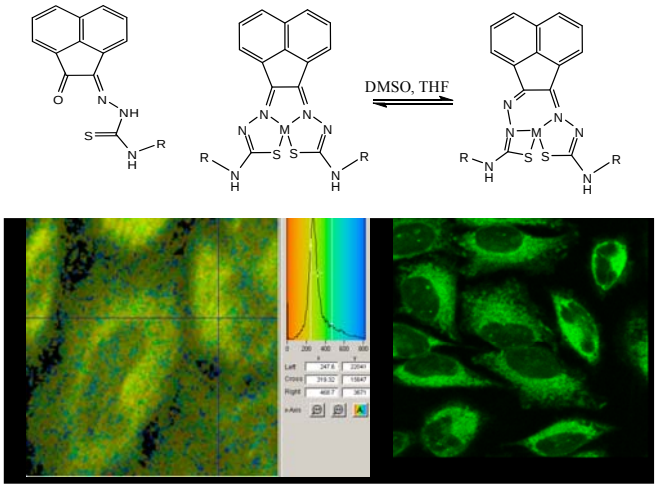

Figure 4: *Representations of the aromatic bis(thiosemicarbazones) studied, and preliminary proof-of-concept FLIM (left) and confocal imaging in HeLa (right) for a Zn(II) analogue*

The symmetric and asymmetric complexes are in exchange in solution as evidenced by ^{1}H NMR techniques and we are now hoping to use fluoresce spectroscopy to identify the nature of the compound when taken up by the cells and whether or not decomposition to free ligand would be observed. The closely related free ligand shown above is only very weakly fluorescent with ca 478 ps lifetime in solution and ca 497 ps lifetime inside the HeLa cell cytoplasm. The confocal fluorescence (λ_{ex} 488/ λ_{em} 543 nm) of the corresponding Zn(II) complex investigated in DMSO showed ca 302 ps lifetime (TCSPC in solution, 50 μM) and strong uptake in HeLa cells with ca 307 ps lifetime inside the cytoplasm (60 mins uptake). We are now studying derivatives with a variety of substituents at the exocyclic nitrogens and exploring the possibility that the Group 13 derivatives localise in the cell nucleus. Our preliminary data suggested that the Zn(II) complex is highly kinetically stable in cells and that this emerging spectroscopic technique may allow us to observe dissociation /decomposition of complexes in cells via emission lifetimes.

Future work: Nuclear targeting complexes for therapy

There is currently much interest in the use of complexes of metallic radionuclides for therapy. A potentially attractive route is to use very short path length Auger electron emission to cause DNA damage however this requires localization of the metal within the nucleus to maximize dose efficiency. This approach has recently been used very successfully for a 111-In complex conjugated to h-EGF protein to target breast cancer and is currently in clinical trials.[4] Currently confirmation of nuclear localization requires lysing and cellular fractionation.

Metal complexes of tridentate thiosemicarbazones

The thiosemicarbazone shown in Figure 5 is in clinical use under the name of Triapine as a broad spectrum anti-tumour agent and its activity is enhanced by coordination to metal ions as an NNS donor.[5] 64-Copper complexes of related thiosemicarbazones have been shown to have high uptake in tumours and have potential as tumour imaging agents.[6] Despite their clinical use there is little known about the speciation of such metal complexes in cells and we have developed some fluorescent analogues to probe their behaviour in cells.[7] These complexes are potent ribonuclease reductase inhibitors[8] and would therefore be expected to localise in the nucleus. The structure of the In complex of a fluorescent quinolyl analogue L which has retained potent cytotoxic behavior is shown in Figure 5

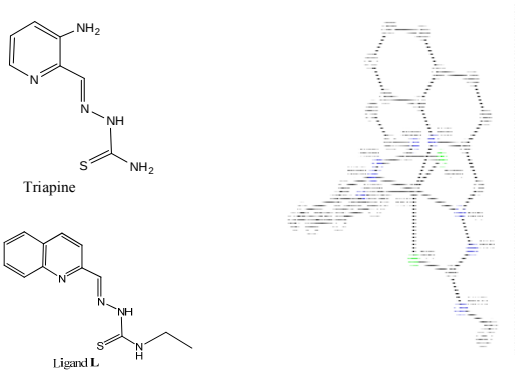

Figure 5*: Structure of Quinolyl ligand* ***L****, Triapine and a fluorescent indium quinolyl complex* InL_2Cl

Preliminary data on these species gathered at RAL suggests that it will be possible to observe dissociation in cells by means of both the wavelength of emission or emission lifetimes. These experiments will be conducted in the next testing sessions at the RAL.

Targeted Metallo-porphyrins

We have recently found that intrinsically fluorescent positively charged indium porphyrin complexes display nuclear uptake without addition of any nuclear targeting agent. Fluorescent images confirm nuclear uptake but do not discriminate between indium complex and free porphyrin. We will now use the change in emission lifetime and differences in emission wavelength between these to confirm if the indium metal is located in the nucleus. Comparison with other porphyrins suggests that the positive charges play an important role in directing the complexes to the nucleus.

Conclusions

Lifetime resolved 2-photon microscopy has clear potential as a tool for investigating the speciation of metal complexes in cells and *in viscera*. Much remains to be done, and we are currently focusing on probing the speciation of these complexes further, and on the development of new methods for image analysis and processing.

Acknowledgements

The Royal Society and the University of Bath are acknowledged for funding SIP and RLA participation in all experiments.

References

1. M. P. S. Dunphy and J. S. Lewis, *J. Nucl. Med.*, **2009**, *50*, 106

2. S. I. Pascu, P. A. Waghorn, B. W. C. Kennedy, R. L. Arrowsmith, S. R. Bayly, J. R. Dilworth, M. Christlieb, R. M. Tyrrell, J. Zhong, R. M. Kowalczyk, D. Collison, P. K. Aley, G. C. Churchill and F. I. Aigbirhio, *Chem.- Asian. J.*, **2010**, *5*, 506

3. S. I. Pascu, P. A. Waghorn, T. Conry, B. Lin, C. James and J. Zayed, *Adv. Inorg. Chem.*, **2009**, *61*, 131

4. K. E. Bailey, D. L. Costantini, Z. Cai, D. A. Scollard, Z. Chen, R. M. Reilly and K. A. Vallis, *J. Nucl. Med.*, **2007**, *48*(9), 1562

5. R. A. Finch, M.-C. Liu, S. P. Grill, W. C. Rose, R. Loomis, K. M. Vasquez, L.-C. Cheng and A. C. Sartorelli, *Biochemical Pharmacology*, **2000**, *59*, 983

6. L. Wei, J. Easmon, R. K. Nagi, B. D. Meugge, L. A. Meyer, and J. S. Lewis, *J. Nucl. Med.*, **2006**, *47*, 2034

7. J. Chan, A. L. Thompson, M. W. Jones and J. Peach, *Inorg. Chim. Acta*, **2010**, *363*, 1140

8. C. R. Chitambar, J. Narasimhan, J. Gay, D. S. Sem, W. J. O'Brien, *Cancer Res.*, **1991**, *51*, 6199

Biocompatible microstructured materials for tissue engineering

Contact *F.Claeyssens@sheffield.ac.uk*

A. A. Gill

University of Sheffield, Materials Science and Engineering Department, Biomaterials and Tissue Engineering Group, Broad Lane, Sheffield, S3 7HQ, United Kingdom

F. Claeyssens

University of Sheffield, Materials Science and Engineering Department, Biomaterials and Tissue Engineering Group, Broad Lane, Sheffield, S3 7HQ, United Kingdom

Introduction

To engineer a complex 3D tissue from cells the production and utilisation of the appropriate 3D scaffold is critical. Cells presented with a flat surface grow typically in a monolayer fashion, while 3D cell cultures can only be achieved via growing them in a 3D micro-environment that is optimally tuned to enhance their adhesion and growth.[1]

Thus the central research question in scaffold manufacture for tissue engineering is; *what specific microstructure and physical properties does a tissue scaffold need to present for optimal cell adhesion/growth?* The main approach is to try to reproduce the microstructure of the Extracellular Matrix (ECM) of a given tissue type. Indeed, the ECM, or the connective tissue between the cells, provides the necessary nanoscale chemical, structural and mechanical environment for a set of cells in a tissue.[2] Although we are still far away from exactly mimicking the ECM by a cell scaffold, important advances have been made in tissue engineering to provide an increasingly detailed substitute for the ECM.

3D tissue scaffolds have been produced as random or ordered microstructured networks. Random 3D networks are produced via *e.g.* solvent casting with particulate leaching, electrospinning or phase separation in combination with freeze-drying/critical point drying[3] while free-form fabrication techniques (such as microstereolithography, μSL) are used to make ordered 3D networks. In general random networks, when compared to ordered structures, are easier to produce in bulk but their microstructure and physical properties are more difficult to control, analyse and interpret. Studies based on scaffolds formed from random 3D networks dominate the current research due to their ease of manufacture when compared to the fabrication of ordered networks. Nevertheless, some recent high-profile studies have indicated a distinct advantage in user-controlled manufacture of 3D structures for tissue engineering. For example, Langer et al. have been able to grow directionally aligned heart muscle tissue for the first time, mimicking natural heart tissue, via using a tissue scaffold with an ordered microstructure.[4] This study showed that the alignment of the heart muscle cells was critically dependent on the specific microstructure of the scaffold.

As indicated by this example; a very important advantage of controlled manufacture of 3D structure via free-form fabrication methods is that a controlled topological environment for cell growth can be provided. Since the 3D structure can be easily adjusted (via changing the structural parameters in a computer aided design (CAD) program), this manufacture platform is ideally suited for exploring the relationship between 3D topology and cell behaviour and to tease out the exact design criteria for scaffolds for different cell and tissue types.

Stereolithography (SL) enables fast prototyping of 3D objects through photopolymerisation. In the photocuring process, a mixture of photoinitiator and reactive prepolymers (monomers or oligomers) is exposed to intense light. The photons are absorbed by the photoinitiator which breaks down and initiates the reaction, forming an insoluble polymer from the prepolymers. The photointitiators used in this experiment break down under UV light, thus in the standard SL set-up UV light is used to polymerise the material via a one-photon process. In one-photon polymerisation (1PP), the polymerisation typically takes place on the surface of the irradiated polymer and the polymerisation depth is governed by the Beers-Lambert law, which limits the in depth resolution. In the writing plane the resolution of this experiment is wavelength-limited and is seldom better than 1 μm.

A novel route to photostructuring is via exploiting 2-photon polymerisation (2PP), where photons of double the wavelength of 1PP are used (typically ~800 nm), so that the photoinitiator needs to absorb 2-photons to break down and initiate the polymerisation. Given that in 2PP absorption cross-section is much smaller much higher intensity light sources need to be used, and typically femtosecond lasers are used to achieve this. This revolutionary production process exhibits important advantages compared to methods based on 1PP, and allows the production of user defined (sub)micrometer definition structures. Indeed, the smallest feature size that has been reported via 800nm 2PP is ~100 nm.[5]

In a former pilot study we have shown that with this set-up we can build 3D structures of 3-4 μm resolution polycaprolactone polymer scaffolds with 2PP.[6] In this study we report a further exploration of 2PP processing of polylactide based polymers.

Both of these polymers are biocompatible, biodegradable and tissue engineering scaffolds produced with these materials provide initial rigidity to an engineered tissue while the tissue builds its own scaffold, *i.e.* the Extracellular Matrix (ECM), and afterwards the engineered scaffold is resorbed by the tissue.

Experimental

In this project we have used a scanning μSL set-up in which focused light is scanned through a liquid photocurable material via a high accuracy xyz-translation stage. The regions which are expose to the light cure or harden, unexposed region remains liquid and can be washed away, resulting in a 3D pattern.

In this project a laser direct write system was constructed which combined a Ti: sapphire laser (Coherent MIRA-900, 810nm, repetition rate 76MHz, pulse width 200fs) focused through a 20x 0.75NA lens (Nikon) with a high precision xyz-translation stage (Aerotech). For the 2 photon-polymerisation an *in house* synthesized photocurable PLA prepolymer (synthesis route described in Ref. 7) was used and this prepolymer 4,4 ′-bis(diethylamino)benzophenone (Sigma-Aldrich) was used as the photoinitiator for two-photon polymerization. The photoinitiator was used at 2 wt % to the pre-polymer.

Structures were created in an automated fashion by creating a program consisting of a series of linear translation instructions (e.g. x+3mm, y+50μm) for the translation stage. Samples were prepared with the resin sandwiched between a glass microscope slide and a 13mm circular glass coverslip separated by two bands of adhesive tape, and the structures written onto the face of the glass coverslip. The glass coverslips were treated with 40mM 3-methacryloxypropyltrimethoxysilane (MAPTMS) in dichloromethane (DCM) prior to use to aid structure adhesion. Indeed, when bare glass coverslips were used the produced microstructures did not adhere to the glass surface and floated off the glass surface during development. When fabrication was complete the samples were developed in toluene to remove uncured monomer and left to dry in air.

The produced structures were used to study the cell growth and attachment of NG108-15 cells, a hybridomal cell line of a rat neuroblastoma and a mouse glioma. This provides us an initial assessment of the neurocompatibility of these scaffolds. The produced structures were briefly sterilized by immersion in IMS

followed by soaking in PBS. NG108-15 Cells were seeded over a range of concentrations and cultured for 48h before being stained for fluorescence imaging.

Results

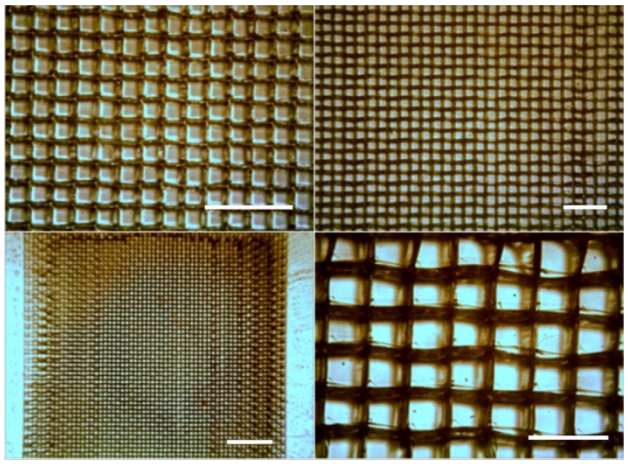

Figure 1: *Optical micrographs of PLA microstructures created by laser direct write Fabricated at a power of 1W and write speed of 5 mm s^{-1}. Scale bars: Top row 200 µm, bottom left 500 µm, bottom right 100 µm.*

Our set of experiments explored the rapid fabrication of macroscopic 3D objects with 2PP. To ensure the polymerization was a true 2PP, we tested polymerizing the prepolymer-photoinitiator mixture under 1W, 810 nm, continuous wave light and no polymerization was observed. Only when the laser was mode-locked properly to provide femtosecond radiation polymerization was observed.

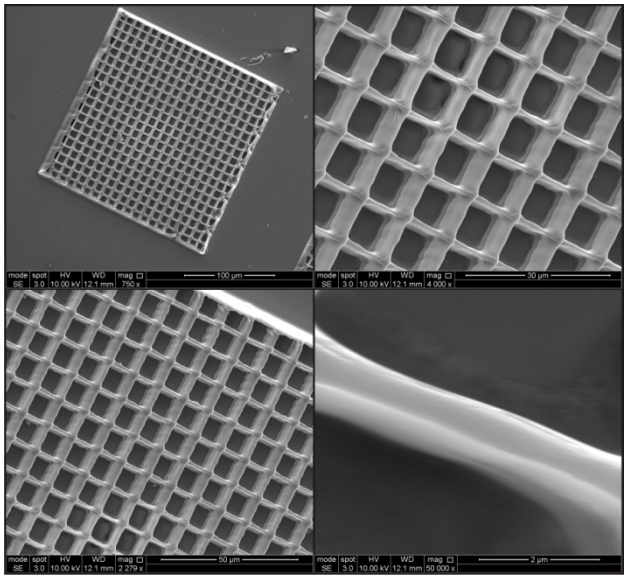

Figure 2: *By expansion of beam filling objective feature resolution was reduced to less than 1µm. Scale bars: Top left 100 µm, top right 30 µm, bottom left 50 µm, bottom right 2 µm.*

A series of experiments was carried out to determine the optimal write speed while fully exploiting the high beam intensity of the laser. Fig. 1 shows the optical microscopy photographs taken of the resulting structures. These structures were written with a beam intensity of 1W and with write speeds of 5 mm s^{-1}, and as shown in Fig. 1 considerably large structures can be achieved in a feasible timescale (5 mins). The line spacing of these cross-hatch structures is 50 µm and the thickness of the individual lines is ~10 µm. An important note is that some of the patterns look distinctly distorted (can be clearly seen in the bottom left in Fig 1). This was mainly attributed to mechanical instabilities during the direct write process and this was largely improved upon during the project.

The thickness of the lines produced is dependent on write speed, beam power and also the cross sectional area of the focal point of the objective. When the back aperture of the objective is filled by the Gaussian-shape laser beam a more defined focal point results giving finer feature resolution. By using a telescopic beam expander (consisting of a 5 cm and a 15 cm lens) to expand the beam a resolution of less than 1 µm was achieved in the xy-direction. The obtained structures are given in Fig. 2, and in this case consist of a 200 µm cross-hatched pattern with line spacings of 10 µm. The resolution in the z-direction is 2~5 µm.

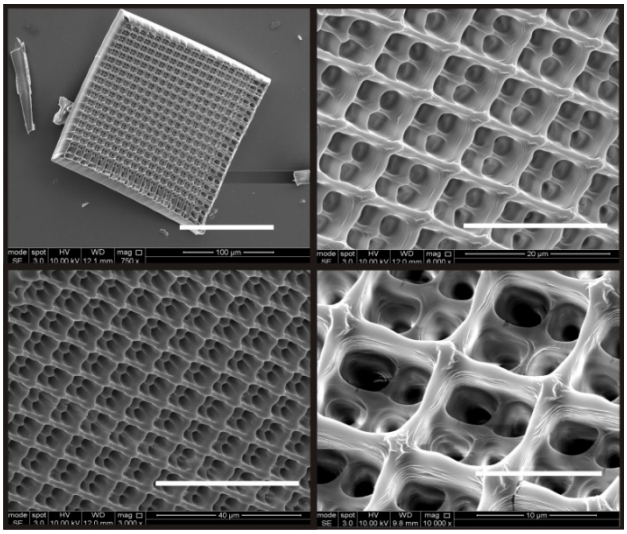

Figure 3: *By writing more than one layer and offsetting the pattern three dimensional porous structures can be produced. Scale bars: Top left 100 µm, top right 20 µm, bottom left 40 µm, bottom right 10 µm.*

An additional feature of 2PP, is that precise 3D microstructuring can be achieved. Indeed, the 2PP technique is up to date the only direct write technique that can deliver 'real' 3D micro- and nanostructuring. During this project we have investigated the possibility of 3D structuring via 2PP, and SEM micrographs of the obtained structures are presented in Fig. 3. In this set of experiments 2 cross-hatched patterns were constructed with a vertical (z-axis) offset by 2 µm and a xy offset of 5 µm (or half the line spacing). One can clearly observe from Fig. 3 that a 3D microporous structure was achieved with this set-up.

These structures, produced by 2PP, have also been studied for neuronal tissue engineering applications. In a first step we assessed the biocompatibility of this particular blend of PLA via studying the viability of human dermal fibroblasts on spin-coated thin films of this material (data not presented). From this data we could conclude that this material proved to be, in general, biocompatible. An interesting question that could be posed now is if the microstucturing can influence cell growth on this material. In particular, our group is interested in using his material for neural tissue engineering. To assess this we cultured neuronal type (NG108-15) cells cultured on 3 sets of produced PLA patterns in a pilot study. The structures consisted of ~10 µm thick lines arranged into 3 mm square grids as detailed before. The patterns produced consisted of an array of squares with lines spaced by 50 µm centre to centre in x and y, an array of rectangles with 50 µm spacing in x as before and a spacing of 150 µm centre to centre in y, and an array of parallel lines with a centre to centre spacing of 50 µm. These patterns were chosen to investigate the effect of microenvironment on

cell growth of these neuronal cells. NG108-15 cells readily align and grow along linear micropattern,[8] while this might not be the case on a square pattern. Indeed, when these cells were seeded on the scaffold and their attachment/growth was investigated after two days in vitro, one can observe that the cells only attached to the parallel lines, and failed to attach to the rectangular and square structures, indicating a degree of shape selectivity in their attachment and growth (see figure 4).

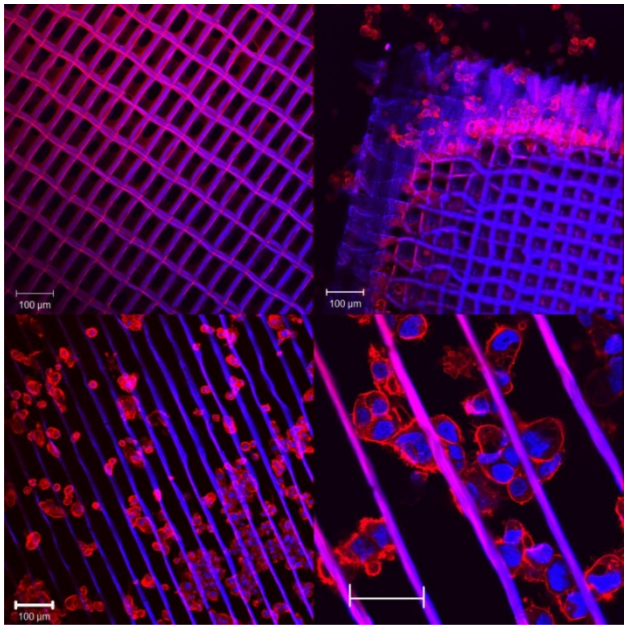

Figure 4: *NG108-15 Cells on Microstructured Surfaces after 48h in culture. Cells have attached successfully to parallel lines of Microstructured PLA however did not attach to square or rectangular structures indicating a degree of surface selectivity. Scale bars top and left, 100 µm, bottom right 10 µm.*

Conclusions

Scanning microstereolithography has been used to create a range of structures with feature resolution as low as 1µm from a photocurable, biocompatible and biodegradable polylactide formulation. The ability to create porous resorbable scaffolds with user defined microstructure was demonstrated, showing the potential of this technology for fabricating structures which mimic the extracellular matrix. Furthermore, it was demonstrated that microstructure can be used to influence cellular behavior, in this case attachment and alignment.

Acknowledgements

The authors thank the EPSRC Laser Loan Pool for the 6 month usage of the Coherent MIRA-900 femosecond laser. The authors would like to thank Dr. Stan Botchway for his support with setting up and servicing the laser during the project. The authors also like to thank Celia Murray-Dunning for cell culture and cell imaging.

References

1. Abbott, A., Cell culture: Biology's new dimension. Nature 2003, 424 (6951), 870-872.

2. Place, E. S.; George, J. H.; Williams, C. K.; Stevens, M. M., Synthetic polymer scaffolds for tissue engineering. Chemical Society Reviews 2009, 38 (4), 1139-1151.

3. Liu, C.; Xia, Z.; Czernuszka, J. T., Design and Development of Three-Dimensional Scaffolds for Tissue Engineering. Chemical Engineering Research and Design 2007, 85 (7), 1051-1064.

4. Engelmayr, G. C.; Cheng, M. Y.; Bettinger, C. J.; Borenstein, J. T.; Langer, R.; Freed, L. E., Accordion-like honeycombs for tissue engineering of cardiac anisotropy. Nature Materials 2008, 7 (12), 1003-1010.

5. Serbin, J.; Egbert, A.; Ostendorf, A.; Chichkov, B. N.; Houbertz, R.; Domann, G.; Schulz, J.; Cronauer, C.; Fröhlich, L.; Popall, M., Femtosecond laser-induced two-photon polymerization of inorganic-organic hybrid materials for applications in photonics. Optics Letters 2003, 28 (5), 301-303.

6. Claeyssens, F.; Hasan, E. A.; Gaidukeviciute, A.; Achilleos, D. S.; Ranella, A.; Reinhardt, C.; Ovsianikov, A.; Xiao, S.; Fotakis, C.; Vamvakaki, M.; Chichkov, B. N.; Farsari, M., Three-Dimensional Biodegradable Structures Fabricated by Two-Photon Polymerization. Langmuir 2009, 25 (5), 3219-3223.s

7. Gill, A.A; Claeyssens, F., 2010, 3D structuring of biocompatible and biodegradable polymers via stereolithography. Methods in Molecular Biology (in press).

8. Schneider, T. W.; Schessler, H. M.; Shaffer, K. M.; Dumm, J. M.; Yonce, L. A., Surface Patterning and Adhesion of Neuroblastoma X Glioma (NG108-15) Cells. *Biomedical. Microdevices* 2001, *3* (4), 315-322.

The plant secretoryome: protein-protein interactions in the higher plant secretory pathway

Contact *chawes@brookes.ac.uk*

Chris Hawes, Anne Osterrieder and Imogen Sparkes, School of Life Sciences, Oxford Brookes University, Oxford, OX3 0BP

Stanley Botchway, Alasdair McKenzie and Andy Ward Central Laser Facility, STFC, Rutherford Appleton Laboratory, Harwell Science & Innovation Campus, Didcot, OX11 0QX

Introduction

The Plant Endomembrane Group at Oxford Brookes has a long history in the study of the structure and function of the higher plant secretory pathway. This is the series of organelles in the cell responsible for the synthesis, processing and packaging of proteins, carbohydrates and lipids that are either sent to the vacuolar system for storage (or other functions) or to the cell surface for exocytosis. Over recent years the group has specialised on *in vivo* imaging and confocal microscopy of the secretory pathway using fluorescent protein constructs. We were the first to describe the motility of leaf Golgi bodies over the cortical endoplasmic reticulum (ER) network (Boevink et al. 1998) This initial success resulted in the award of a number of BBSRC grants looking at protein transport between the ER and Golgi and the nature of the ER export sites. Photobleaching technology has been used to characterise the transport of membrane proteins between the two organelles and recently the novel concept of the Golgi apparatus and the ER export sites working in tandem as unified complexes moving over or in the ER membrane has been published (Brandizzi *et al.* 2002, daSilva *et al.* 2004, Runions *et al*. 2006). This raises the intriguing question as to how individual Golgi bodies manage to stay tethered to the ER and yet to maintain the integrity of the stack whilst being propelled along the ER.

The successful functioning of the plant secretory pathway is also dependent on the sequential interactions of a myriad of proteins each with a defined task. Unraveling the interactions between various sub-sets of these proteins is a main goal of our research programme, which also involves a number of national and international collaborations.

This report summarises a series of experiments that were carried out to investigate the interactions between plant Golgi matrix proteins and regulatory GTPases (Latinjnhouwers et al 2005) as a continuation of the work reported in the CLF annual report 2006-2007. We have also carried out a series of experiments to investigate potential heteo-and homo-dimerisation of plant reticulon proteins that are responsible for maintaining the curvature of endoplasmic reticulum tubules

Protein Interactions at the plant Golgi apparatus

Golgins are large coiled-coil domain proteins and in animal cells it has been shown that they can dimerise or interact with other golgins to carry out tethering functions within the secretory pathway. Therefore GFP fusions of AtCASP or GC2 (a homologue of the animal golgin-84 predicted to be located at the *cis*-Golgi) respectively were expressed on their own to determine their lifetime and the obtained GFP lifetimes were compared to the ones of GFP co-expressed with mRFP fusions of the same protein. No significant reductions in GFP lifetimes were observed for the combinations GFP-AtCASP with mRFP-CASP and GFP-GC2 with mRFP-GC2. In a previous study we had determined that GFP-AtCASP and mRFP-GC1 did not appear to interact *in vivo*. Therefore we now tested GFP-AtCASP with mRFP-GC2 but did not observe any interaction either. This indicates that the functions and tethering mechanisms of plant golgin homologues might work in a different manner compared to their counterparts in animal cells.

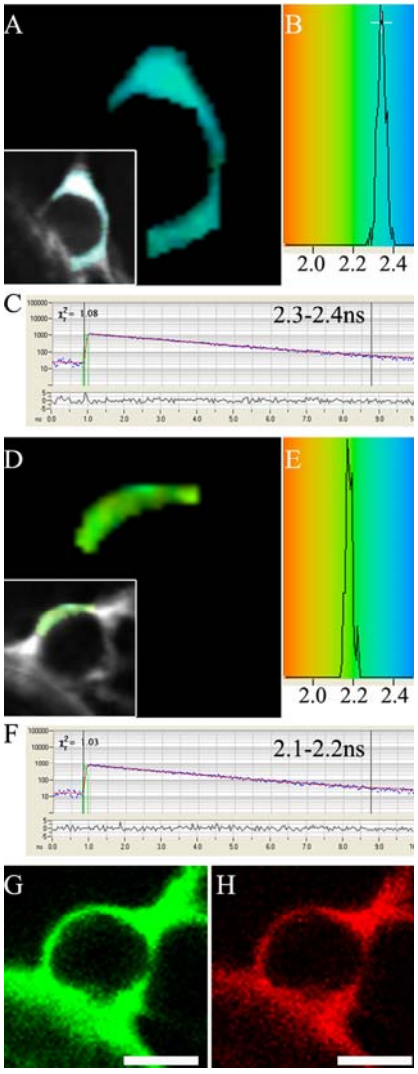

Figure 1. FRET-FLIM analysis of RTNLB1 dimerisation in tobacco leaf epidermal cells. RNLB1-eGFP (A-C) and coexpression with mRFP-RTNLB1 (D-H) in tobacco leaf epidermal cells were tested for interaction through FRET-FLIM. A region of interest on the ER continuous with the nuclear envelope was selected (A,D, see inset) based on the lifetime decay curves of points within the region having a χ^2 value between 0.9-1.4 (C,F). The lifetimes of the points within the selected region are displayed (B,E) and psuedocoloured accordingly in A and D. Confirmation of coexpression of eGFP and mRFP RTNLB1 fusions are shown (G,H). The lifetime of the combination is more than 0.1ns lower than the donor fusion alone, indicating RTNLB1 dimerisation. Scale bar 5μm.

Many mammalian golgins also bind to small regulatory GTPases. These interactions are thought to be required for the correct Golgi stack localisation of golgins as well as for trafficking and membrane tethering events. We have previously proved this to be true for some *trans*-Golgi golgins ((Hawes & Osterrieder 2007, Osterrieder et al. 2009). We now tested GFP fusions of the *cis*-Golgi located Golgins AtCASP, GC1 and GC2 with mRFP fusions to the small plant GTPases RabD2A, RabB1b, Rab-H1^{b} and Rab-H1^{c}. Surprisingly, no significant decrease of GFP lifetimes was observed for any of the combinations, which suggests that these proteins might employ different Golgi targeting mechanisms or might interact with other small GTPases than the ones studied in this screen. Further work is being undertaken with other *cis*-Golgi golgins such as p115.

Protein interactions in at the plant endoplasmic reticulum

The endoplasmic reticulum (ER) is the key organelle for producing and processing proteins for storage or export from the cell. As part of an on going project to investigate the organisation of the cortical ER network we have been studying the role of the reticulon family of proteins in inducing curvature of the ER network (Sparkes et al. 2010). We have demonstrated that these proteins are restricted in distribution to membrane tubules and curved edges of cisternae and not to the faces of cisternal sheets. One hypothesis is that they form a "W" shaped wedge in the ER membrane and either hetero- or homodimerise or oligomerise to induce curvature. Interactions of various combinations of reticulons and truncated forms were measured by FRET/FLIM in cortical epidermal cells of tobacco leaves, after transient expression of green and red-fluorescent protein tagged constructs (Sparkes et al. 2010). The average of the range of pairs of constructs expressed indicated at least a 0.2 ns decrease in lifetime of the pairs compared to the control donor expressed alone. Therefore, all combinations of full-length RTN and truncations tested appeared to show some degree of oligomerisation.

Development of Laser Tweezers on a TIRF microscope

Our initial attempts at TIRF microscopy gave totally unexpected results (Hawes et al. 2010). In theory the presence of the cell wall in plant tissue precludes the use of TIRF as a

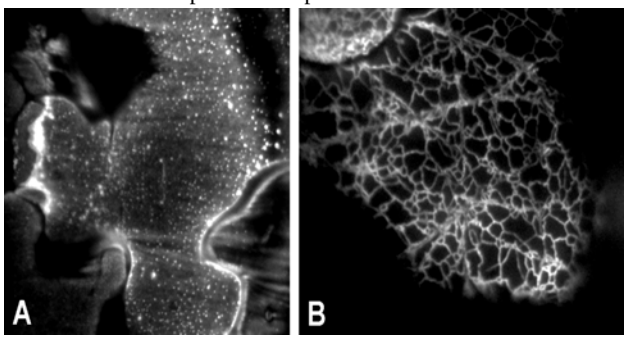

Figure 2. A. TIRF image of the plasma membrane of a tobacco leaf epidermal cell expressing GFP-LTI6B showing punctae and a filament associated with the PM (image courtesy of A. Martiniere). B. TIRF image showing cortical endoplasmic reticulum in a similar cells labelled with GFP-HDEL.

viable technique. However, in our first trial runs stunning images of protein location on the plasma membrane, of cortical ER and Golgi bodies were obtained. We assume that this is due to the cell wall having a similar refractive index to coverslip glass and thus the evanescent wave occurs at the wall/plasma membrane interface (Hawes et al. 2010). This has opened up a whole new range of experiments on secretion to the plasma membrane. As a result of these data it was decided to build laser tweezers into a TIRF microscope rather than the confocal attached to the two photon FLIM set up. This is based around a Nikon TE-200-S inverted TIRF microscope with a 1.49NA oil immersion objective. Imaging is carried out with a 473nm diode laser and trapping with a 1064 Nd:YAG diode laser focussed to the imaging plane of the microscope. This development work has been carried out by Dr Andy Ward and a sandwich student Alasdair McKenzie and the first successful trapping of fluorescent beads has just been carried out prior to experiments being undertaken on the trapping of Golgi bodies in tobacco and arabidopsis leaves.

Conclusions

Work on the interactions of Golgi matrix proteins with small regulatory GTPases and with each other is on going, further combinations of proteins are to be tested. FRET/FLIM can be used to study self interactions of proteins on the endoplasmic reticulum and this work will be extended to cover interactions of ER-plasma membrane anchor point proteins as they are identified in other projects. TIRF is a technique that can be used with plant tissues and as such opens up a new avenue for studying interactions at the plasma membrane. Also the major components of the cortical endomembrane system can be imaged which will permit the use of a combination of laser trapping and TIRF microscopy to manipulate organelles such as the Golgi apparatus.

Acknowledgements

Part of this work was funded by a BBSRC Grant No. BB/F008147/1 to CH.

References

Boevink, P., Oparka, K., Santa Cruz, S., Martin, B., Betteridge, A. & Hawes, C.R. (1998). Stacks on tracks: the plant Golgi apparatus traffics on an actin/ER network. Plant Journal. 15, 441-447.

Brandizzi, F., Snapp, E., Roberts, A., Lippincott-Schwartz, J. & Hawes, C.R. (2002). Membrane protein transport between the ER and Golgi in tobacco leaves is energy dependent but cytoskeleton independent: evidence from selective photobleaching. Plant Cell 14, 1293-1309.

Hawes, C., Evans, D. & Runions, J. (2010). A green revolution – getting the measure of a plant cell. The Biochemist 32, 8-11.

Hawes, C.R.. & Osterrieder, A. (2007). *In vivo* interactions of higher plant Golgi matrix proteins by fluorescence life-time imaging. Central Laser Facility Annual Report 2006/7 105-106.

Osterrieder, O., Carvalho, C.M., Latijnhouwers, M., Johansen, J.N., Stubbs, S., Botchway, S. & Hawes, C. (2009). Fluorescence lifetime imaging of interactions between Golgi tethering factors and small GTPases in plants. Traffic 10, 1034-1046.

Runions, J., Brach, T., Kühner, T. & Hawes C. (2006). Photoactivation of GFP reveals protein dynamics within the endoplasmic reticulum membrane. J. Exp. Bot. 57, 43-50.

Da Silva, L.L.P., Snapp, E.L., Denecke, J., Lippincott-Schwartz, L., Hawes, C. & Brandizzi, F. (2004). Membrane cargo-mediated recruitment of GTPase Sar1p to specific export sites of the ER membrane. Plant Cell 16, 1753-1771.

Sparkes, I., Tolley, N., Aller, I., Svozil, J., Osterrieder, A., Botchway, S., Mueller, C., Frigerio, L. & **Hawes, C.** (2010). Five plant reticulon isoforms share ER localisation, topology, ER membrane shaping properties and the ability to form both homo- and heterotypic interactions. Plant Cell 22, 1333-1343.

Supra-molecular rules in signalling networks: A single molecule comparative study in cells and tissues

Contact *Marisa.Martin-Fernandez @stfc.ac.uk*

David T. Clarke
STFC-Central Laser Facility
Research Complex at Harwell

Michael Hirsh
STFC-Central Laser Facility
Research Complex at Harwell

Marisa Martin-Fernandez
STFC-Central Laser Facility
Research Complex at Harwell

Sarah R. Needham
STFC-Central Laser Facility
Research Complex at Harwell

Selene K. Roberts
STFC-Central Laser Facility
Research Complex at Harwell

Daniel J. Rolfe
STFC-Central Laser Facility
Research Complex at Harwell

Christopher J. Tynan
STFC-Central Laser Facility
Research Complex at Harwell

Stephen E.D. Webb
STFC-Central Laser Facility
Research Complex at Harwell

Martyn Winn
STFC-Computational Sciences and Engineering
Daresbury Laboratory

Introduction

We have developed single molecule and other fluorescence techniques on the Octopus facility, combined with simulation, modelling and analysis techniques as part of a programme in the Lasers for Science Facility (LSF). Our first aim is to define patterns of conformation association, activation and signal transduction for the 4 members of the ErbB family and their correlation with plasma membrane proximal receptor traffic and signalling using cultured cells. We also aim at deriving models of ligand-induced behaviour using single molecule and ensemble FLIM and systems predictions and to establish how this is influenced by feed-back loops and perturbations. By testing these models on primary epithelial cells and tissues we will adapt the models iteratively to create a framework of response prediction for the network. Our ultimate goal is to derive probes and/or algorithms based on the models, suitable use with fixed or fresh human tissues to determine model robustness and network predictability in this real world setting.

Signal transduction by the ErbB receptor family

The ErbB receptor family are ubiquitously expressed growth factor-binding proteins that belong to subclass I of the superfamily of receptor tyrosine kinases (RTKs) [1]. This receptor family has four members (ErbB1-4); excessive signalling by these receptors upsets the balance between cell growth and apoptosis resulting in the development of a wide variety of solid tumours, including lung, mammary carcinoma, glioblastomas and squamous carcinoma [2]. In adulthood, insufficient signalling by this receptor family is linked to the development of neurodegenerative disorders, such as multiple sclerosis and Alzheimer's disease [reviewed in 3].

The receptors in the ErbB family have in common a structure (Fig. 1) consisting of an extracellular growth factor-binding domain (ectodomain), a single transmembrane alpha-helix, and a cytoplasmic domain containing a tyrosine kinase region, which is flanked by juxtamembrane (~40 residues) and C-terminal regulatory regions [1]. Upon binding their respective growth factors, the role of the ErbB receptor family is to transduce this signal across the plasma membrane by initiating the catalytic activity of their intracellular kinase [3]. This is a poorly understood mechanism shown to be associated with the formation of almost every possible pair-wise combination of homo- and heterodimers (and perhaps larger oligomers) of the receptors in this family [4]. ErbB signals are terminated through the endocytosis of the receptor-ligand complex [5] (Fig. 1). Downstream intracellular signalling pathways are then initiated via the recruitment of a large repertoire of adaptors, enzymes and transcription factors, which activate the gene programmes that control cell proliferation, survival, adhesion, migration and differentiation [reviewed in ref.6].

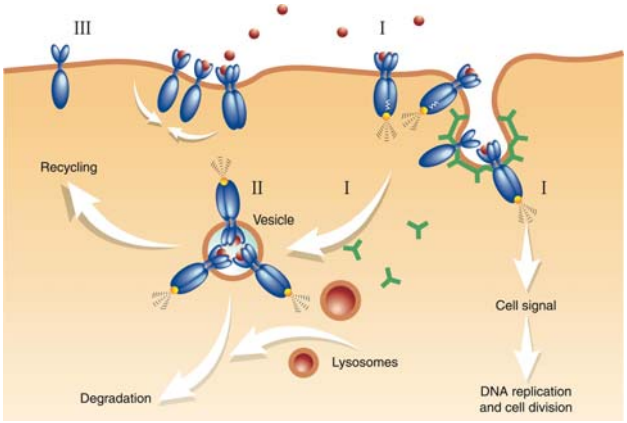

Figure 1. ***Schematic of receptor endocytosis.*** *Receptors bind ligand at the cell surface (I) and are transported along the plasma membrane towards clathrin-coated pits to be internalised in vesicles (II). Then ligand-bound receptors are targeted for degradation in acidic intracellular conpartments (lysosomes) or recycled to the cell surface. Endocytosis is used by the cell to downregulate receptor signals. It is common to find in cancerous cells the recycling pathway potentiated. [9]. All receptors in the EGFR family are endocytosed with the exception of ErbB2, which escapes endocytosis and, as a result, is the most oncogenic member of this receptor family.*

Using single molecule fluorescence microscopy to study structure-function relationships in ErbB receptor signalling

Predictions from 3-D structures need to be tested and verified by experimental evidence from ErbB receptor molecules in the physiological environment of the cell. Unlike crystallised receptor fragments, intact receptors in cells are influenced by glycosylation, and by the plasma membrane's action potential, hydrophobic environments, 2-D geometrical restrictions and local curvature [7,8]. Interactions with other transmembrane receptors and/or intracellular substrates might also play an important role in the regulation of ErbB activation, as well as heterodimerisation, ligand-independent lateral propagation of activation via transient dimerisation and the formation of receptor oligomers [9,10]. These interactions are not explained by the structural data available and cannot be fully investigated either by ensemble fluorescence imaging technologies because these rely on non-physiological, and often ineffectual synchronisation of events, hence being inadequate to characterise conformational changes associated to signalling as the information can be lost in the ensemble average.

Single molecule fluorescence microscopy techniques can bridge the areas of structural biology and cell imaging by yielding constraints that have allowed us to derive *in situ* receptor structural information during signal transduction in cells [11]. To gain information on protein interactions and conformational changes it is necessary to resolve distances on the order of the size of the receptor. These can be accessed by using single pair FRET (spFRET). FRET is a phenomenon by which the excited-state energy of an optically excited molecule (donor) is transferred to a neighbouring molecule (acceptor) nonradiatively via intermolecular dipole coupling in the range 1-8 nm, a length-scale encompassing the typical diameter of membrane proteins [12]. Crucially, spFRET and single molecule fluorescence polarisation (smFP) can be measured simultaneously because the emission polarisation ratio of a single molecule is independent of the means of excitation, hence the acceptor/emission polarisation ratios can also be recorded after FRET excitation [13].

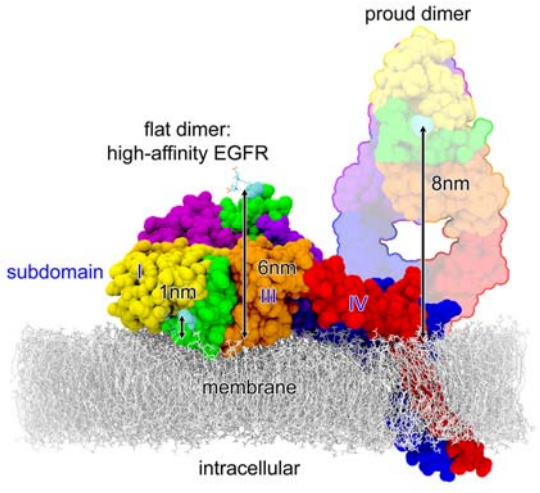

Figure 2. ***The back-to-back dimer of ErbB1 coloured by domain.*** *The ErbB1 cognate ligand, the epidermal growth factor (EGF), is depicted in green. Subdomains I-IV of the ErbB1 receptor are numbered in the figure. The model is obtained from combining crystal structures as described in [14]. The figure shows the two possible orientations of the EGFR ectodomain dimer revealed by single molecule and FLIM-FRET microscopy. The two conformations are associated to the two different affinities shown by ErbB1 to its ligand.*

The challenge of single molecule fluorescence imaging in mammalian cells

Single-molecule data on protein conformational changes in cell-free environments are much easier to quantify in the absence of out-of-focus cell autofluorescence. Total internal reflection (TIR) excitation allows the rejection of most, but by no means all out-of-focus background. This results in an unavoidable further reduction in signal-to-noise in the single molecule images from cells, which is even more acute when photons have to be split into different channels to collect spFRET and smFP data, where the signal is partitioned into four components discriminated in two colours and two polarisations to derive *in situ* protein structure [15]. In addition, as a side effect of TIR, fluorophores located at varied axial distances, as with proteins in the plasma membrane, experience different excitation field strengths. The fluorescence from single-molecules can therefore have a wider spread of signal-to-noise ratios than biomolecules immobilized on the same glass surface exposed to the same incident intensity. Using current image analysis technology we have successfully analysed data from those features bright enough to be easily distinguished from the background, but have had to discard significant amounts of potentially useful data.

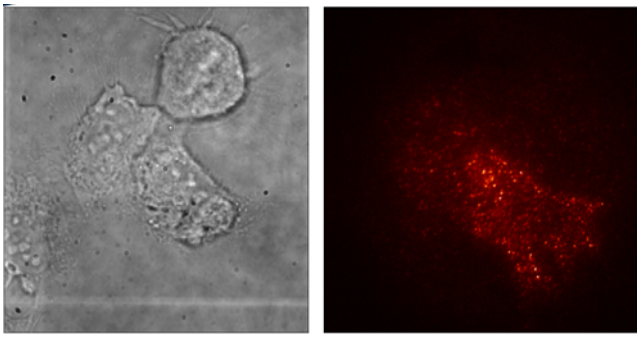

Figure 3. *Wide field transmission (left) and single molecule fluorescence (right) images of HeLa cells. The EGFR molecules at the cell surface were labelled with EGF tagged with the red emitting fluorophore Atto647. The spots on the figure on the right show the location of single EGF/EGFR complexes in different oligomerisation stages. The number of fluorophores is determined by the number of photobleaching steps in each spot [15].*

Using a Bayesian approach, pre-existing knowledge of the subject being measured and of the experimental apparatus used to make the measurements is explicitly included in the analysis, creating a much more powerful algorithm with trustworthy results where the limits of the analysis are clearly understood. This is in contrast to traditional ad-hoc methods where assumptions are often implicit and not appreciated by some who use them. Available prior knowledge has not yet been effectively included in the analysis of single molecule data, which in live cells leads to poor detection rates and crucially, to potentially erroneous conclusions. Additionally, every inferred result from a Bayesian analysis is accompanied by a confidence limit. This combination of increased detection rate and quantitative results make Bayesian techniques the optimal method to be applied to the analysis of spFRET and smFP data in live cells [16,17]

Ongoing experiments

We are currently choosing a preferred cell model(s) among a pool of ErbB1-4 expressing lung and breast cancer cell lines by screening their suitability to single molecule investigations. The best model should allow the study of heterocomplexes of all 4 receptors and mutant versions at single molecule level. We are also producing intracellular and extracellularly-tagged ErbB1-4 and cell lines expressing at least two receptor members to investigate combinatorial ErbB oligomerisation. We have begun

to use FRET to investigate ErbB1-ErbB2 interactions using fluorescent ligands and fused fluorescence proteins as probes which will be soon extended to ErbB2-ErbB3 complexes. We have also developed a method that enables single molecule nanoimaging in the X,Y plane of inter-molecular distances with <10 nm resolution in physiological conditions, bridging the gap between Forster Resonance Energy Transfer (FRET) and optical resolution. Its application allowed measurement of the much sought after distances between epidermal growth factor receptors predicted by dimer structures but too large for FRET. We are also investigating the effect of disrupting ErbB intracellular interactions with lipid rafts, actin, and microtubules on ErbB receptor oligomerisation and recruitment of SHC-GFP to the oligomers in HeLa cells. Finally, we are commissioning a 5-colour single molecule microscope to investigate the formation of macro-molecular complexes at the plasma membrane of living cells.

Conclusions

Pushing the frontiers of our understanding of signalling networks in the true physiological context requires a multidisciplinary approach. In this LSF programme we are utilising the sample preparation methods, fluorescence microscopy techniques and data analysis and simulation methods within the Octopus facility at the ensemble and single molecule levels to shed light on receptor structure-function relationships and interactions during signalling in cells. The ErbB receptor signalling network best exemplifies the significance of aberrations in the development of some of the most potent human malignancies. The further development of single molecule methods applicable to mammalian cells may reveal the alternative molecular mechanisms that ensure outputs in the de-regulated disease state, leading to a better understanding of positive and negative feed-back mechanisms used by cells to by-pass therapies.

Acknowledgements

The authors gratefully acknowledge the support by the Biology and Biotechnology research council (grant number BB/G006911/1).

References

1. Yarden, Y. The EGFR family and its ligands in human cancer: signalling mechanisms and therapeutic opportunities. *Eur. J. Cancer* 2001;S3-S8.
2. Yarden, Y. and Sliwkowski M.X.. Untangling the ErbB signalling network. *Nat. Rev. Mol. Cell Biol.* 2001;2:127-137.
3. Bublil EM and Yarden Y.. The EGF receptor family: spearheading a merger of signaling and therapeutics. *Curr. Opin. Cell Biol*. 2007; 19 (2): 124–134.
4. Tzahar E., Waterman H., Chen X., Levkowitz G., Karunagaran D., Lavi S., Ratzkin B.J. and Yarden Y.. A hierarchical network of interreceptor interactions determines signal transduction by Neu differentiation factor/neuregulin and epidermal growth factor. *Mol. Cell. Biol.* 1996; 26 16: 5276.
5. Wiley, S.H. Trafficking of the ErbB receptors and its influence on signalling. *Exp. Cell. Res.* 2003; 284:78-88.
6. Singh A.B. and Harris RC. Autocrine, paracrine and juxtacrine signaling by EGFR ligands. *Cellular Signalling* 2005; 17: 1183-93.
7. Citri A., J.Gan, Y. Mosesson, G. Vereb, J. Szollosi, Y. Yarden. *Embo Reports* 2004; 5: 1165. 17.
8. Defize, L.H.K. J. Boonstra, J. Meisenhelder, W. Kruijer, L. G. J. Tertoolen, B. C. Tilly, T. Hunter, E M. P. van Bergen en Henegouwen, W. H. Moolenaar, and S. W. de Laat. Signal transduction by epidermal growth factor occurs through the subclass of high-affinity receptors. *J. Cell Biol*. 1989; 109:2495-2507.
9. Winstanley J. Cooke T, Murray G.D., Platt-Higgins A., and Rudland P.S. The long term prognostic significance of c-erbB-2 in primary breast cancer. *Brit. J. Cancer*.1991; 63, 447-450.
10. Fleishman SJ, Schlessinger J, Ben-Tal N. A putative molecular-activation switch in the transmembrane domain of erbB2. *Proc. Nat. Acad. Sci*. 2002; 99: 15937-15940.
11. Webb, S.E.D., S.K. Roberts, S.R. Needham, C.J. Tynan, D.J. Rolfe, M.D. Winn, R. Barraclough, D.T. Clarke, and M.L Martin-Fernandez. Single molecule imaging and FLIM show different structures for high and low-affinity EGFRs in A431 cells. *Biophys. J.* 2008; 94:803-819.
12. Stryer, L., and R.P. Haugland. 1967. Energy transfer: a spectroscopic ruler. *Proc. Natl. Acad. Sci. USA*. 58:719–726.
13. Forkey J., M. E. Quinlan, M. A. Shaw, J.E.T. Corrie & Y.E. Goldman. Three-dimensional structural dynamics of myosin V by single-molecule fluorescence polarisation. *Nature* 2003; 422:399-404.
14. Kaestner J., H.H Loeffler; S. K. Roberts, M. L. Martin-Fernandez, and M. D Winn. Ectodomain orientation, conformational plasticity and oligomerization of ErbB1 receptors investigated by molecular dynamics. *Journal of Structural Biology* (2009).167(2):117-128.
15. Webb, S. E. D., Needham, S. R., Roberts, S. K., Rolfe, D. J., Clarke, D. T. McLachlan, C. I., Hobson, M. P. and Martin-Fernandez, M. L. Simultaneous widefield single molecule orientation and FRET microscopy in live cells. *Optics Express* 2008; 16: 20258.
16. Mashanov, G. I., Molloy, J. E., Automatic detection of single fluorophores in live cells. *Biophys. J.* 2007; 92:2199-2211.
17. Sergé, A., Bertaux, N., Rigneault, H., Marguet, D., Dynamic multiple-target tracing to probe spatiotemporal cartography of cell membranes. *Nature Methods* 2008; 5:687-694.

The role of BER proteins in the repair of DNA damage induced following NIR multiphoton laser microbeam irradiation

Contact *Pamela.Reynolds@rob.ox.ac.uk*

P. Reynolds
Gray Institute for Radiation, Oncology & Biology,
University of Oxford, ORCRB, Roosevelt Drive, Oxford, OX3 7DQ

S. L. Cooper
Gray Institute for Radiation, Oncology & Biology,
University of Oxford, ORCRB, Roosevelt Drive, Oxford, OX3 7DQ

P. O'Neill
Gray Institute for Radiation, Oncology & Biology,
University of Oxford, ORCRB, Roosevelt Drive, Oxford, OX3 7DQ

S. W. Botchway
Central Laser Facility, Rutherford Appleton Laboratory, Harwell Science and Innovation Campus, Didcot, OX11 0QX

A. W. Parker
Central Laser Facility, Rutherford Appleton Laboratory, Harwell Science and Innovation Campus, Didcot, OX11 0QX

Introduction

Deoxyribonucleic acid (DNA) is continually undergoing DNA damage and repair. DNA damage can arise from both endogenous and exogenous sources. Exogenous DNA damage occurs following exposure to ionising radiation. A specific feature of ionising radiation is the production of clustered DNA damage; when two or more lesions form within one to two helical turns of the DNA. It has previously been shown that these clustered lesions have reduced repairability compared to individual lesions (1, 2). Unrepaired DNA lesions can ultimately lead to chromosome aberrations mutations and possibly cancer therefore mammalian cells have developed highly conserved DNA repair pathways to repair damaged DNA.

The repair of damaged base lesions occurs predominantly via base excision repair (BER [Fig. 1]). Recognition of the damaged base occurs by a DNA glycosylase which cleaves the N-glycosidic bond to create an apurinic or abasic site (AP site). The DNA backbone is then cleaved by an AP endonuclease creating a single stranded nick 5' to the AP site (3). The repair can then progress through either short patch-BER (SP-BER) or long patch-BER (LP-BER) (Fig.1, (4)). In SP-BER, XRCC1 is recruited rapidly to the nick and acts as a scaffold protein for polymerase β (Pol β) and Ligase III (5). Pol β inserts the missing base and cleaves the 5' phosphate to allow ligation by Ligase III. When Pol β is unable to cleave the 5' phosphate, BER proceeds by LP-BER. During LP-BER, Pol δ or Pol ε is recruited to insert bases in a proliferating cellular nuclear antigen (PCNA) dependent manner, which results in DNA strand displacement (Fig. 1 (3)). Flap structure specific endonuclease 1 (FEN1) cleaves the DNA flap to create a ligatable structure before ligation occurs by Ligase 1 (3).

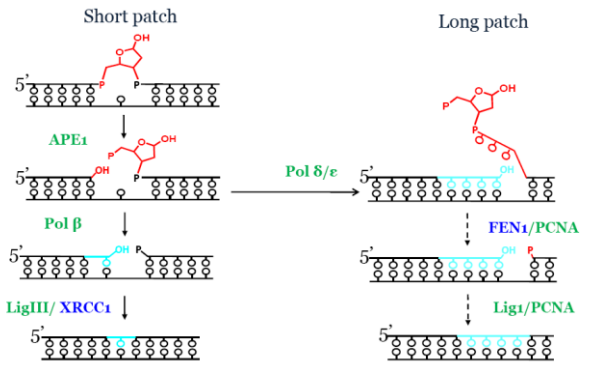

Figure 1: Schematic diagram representing the repair of base lesions by BER.

Previously we have shown that NIR laser microbeam irradiation induces DNA double strand breaks of different complexity (6, 7). Our initial studies demonstrate that following irradiation, base lesions are induced within the DNA and recruit proteins involved in both SP-BER and LP-BER (represented by the recruitment and loss of XRCC1-YFP and FEN1-GFP respectively). Clustered DNA damage is known to be repaired in part by LP-BER. We interpret the different repair kinetics in terms of the repair of single strand breaks (SSBs) and SSBs in clustered damage sites processed by SP- and LP-BER.

Methods

Cell culture

EMC11 (XRCC1$^{-/-}$) cells were cultured in Dulbecco's modified minimum essential medium (DMEM) supplemented with 10% foetal calf serum (FCS), 100 µg/ml penicillin streptomycin and 2mg/ml L-glutamine at 37ºC with 5% CO_2 in air.

Transient transfection of EMC11 cells

EMC11 cells were plated at 2 x 10^5 cells per 30 mm glass bottom dishes 24 h prior to transfection. Cells were transfected with 5 µg of XRCC1-YFP (a gift from Dr. G. Dianov) or FEN1-GFP (Insight Biotechnology, UK) DNA according to the Qiagen SuperFect® transfection reagent protocol. In brief, 5 µg of DNA was added to a total volume of 100 µl OptiMEM. SuperFect® transfection reagent (15 µl) was added for 5-10 min followed by the addition of 600 µl of complete culture medium. The transfection reagent was added to the cells and incubated for 3 h. The transfection reagent was removed by washing 3 x in 1 ml phosphate buffer saline and cells were incubated for 24 h prior to irradiation.

Laser set-up

A Ti:Sa laser (Mira 900, Coherent Inc., USA) tuned to 730 nm was focused through a x 60 water microscope objective, numerical aperture 1.20 of an inverted microscope (TE2000, Nikon). A customised computer software programme (LabView™) operated the automated microscope stage in the x- and y-plane at a step size of 16 µm.

Real time NIR multiphoton laser microbeam irradiations.

Cells were incubated with 10 µg/ml Hoechst dye for 10 min prior to irradiation at 37°C. A red bandpass filter (RG610) was placed on top of the culture dish to prevent the Hoechst dye from absorbing UV light from ambient light. Cells were maintained at 37°C throughout the irradiation using the temperature control chamber connected to a pumped water circulator (Neslab RTE7 Digital One, Thermo Scientific). The laser was set to a wavelength of 730 nm and a nominal power of 10 mW measured through the x 40 air, numerical aperture

0.95, microscope objective. Cells were irradiated in culture medium using a x 60 water objective. Time 0 was recorded immediately following irradiation of the cells (less than 10 s) and images were collected at the stated times following irradiation using confocal microscopy (EC1, Nikon) equipped with an argon ion laser at 488 nm. The images were collected using three Kalman filtered scans with a minimum of 10 cells visualised for analysis per experiment.

Results

Real time kinetics of recruitment and loss of XRCC1-YFP to DNA damage induced by NIR multiphoton laser microbeam irradiation

Cycling EMC11 cells transiently transfected with XRCC1-YFP were irradiated using the NIR laser microbeam to determine the real time recruitment and loss of XRCC1-YFP at sites of DNA damage. XRCC1-YFP is rapidly recruited to sites of DNA damage reaching maximal levels within 2-3 min (Fig. 1 inset). The level of XRCC1-YFP fluorescence is 30% of the maximal fluorescence at 60 min following irradiation. At 240 min, a residual relative fluorescence level of 15% was determined. The repair of NIR laser microbeam induced lesions occurs with bi-exponential decay kinetics. The majority of repair (70%) occurs via a fast component with a half-life of 14 ±6 min. A small component (30%) is repaired with a significantly longer half-life of 230 ±175 min.

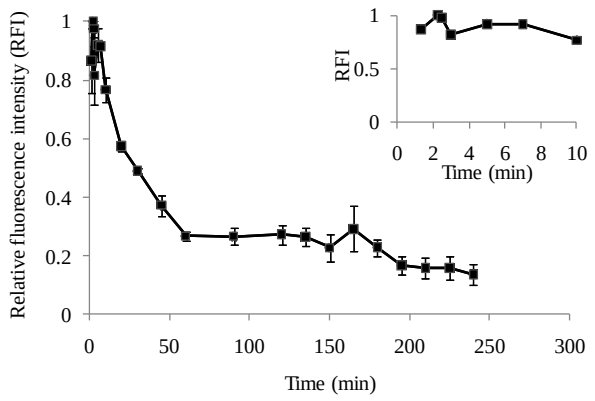

Figure 2: Real time recruitment and loss of XRCC1-YFP fluorescence to sites of DNA damage following NIR multiphoton laser microbeam irradiation. The inset represents the data expanded to show the first 10 min in more detail. Each point represents the normalised relative fluorescence intensity of a minimum of 10 cells per experiment and the mean of 3 independent experiments ± SEM.

Real time kinetics of recruitment and loss of FEN1-GFP following NIR laser microbeam irradiation

Cycling EMC11 cells were transiently transfected with FEN1-GFP and irradiated using the NIR multiphoton laser microbeam. Following irradiation, FEN1-EGFP is rapidly recruited to sites of induced DNA damage. Maximal relative fluorescence was seen later than that of XRCC1-YFP (~2 min) at ~5 min following irradiation (Fig. 3 inset). Within 15 min, FEN1-GFP relative fluorescence intensity is 15% of the maximum fluorescence. FEN1-GFP reaches background fluorescence intensity levels within 60 min following irradiation (Fig. 3). The repair of induced lesions involving FEN1-GFP is readily fitted by a single exponential decay with a half-life of 15 ±2 min. this value is similar to that seen with XRCC1-YFP.

Discussion

The data presented show that following NIR multiphoton laser microbeam irradiation key proteins involved in SP-BER (XRCC1-YFP) and LP-BER (FEN1-GFP) are recruited to sites of induced DNA damage. XRCC1-YFP is involved in the repair of NIR multiphoton laser microbeam induced damage with bi-exponential repair kinetics suggesting that repair occurs by two distinct processes. It is suggested that the fast component of repair represents repair of less complex DNA damage which is consistent with SP-BER repair of simple DNA lesions (Fig. 4). This is consistent with previous investigations by Dikomey and Franzke (8) that showed that DNA strand break repair occurs with three distinct half-lives (Table 1). The fast

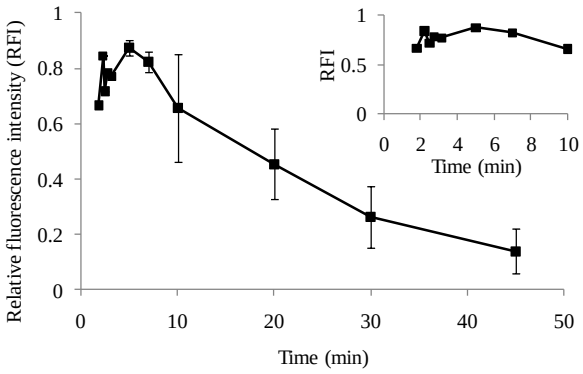

Figure 3: Real time recruitment and loss of FEN1-GFP fluorescence following NIR multiphoton laser microbeam irradiation. The inset represents the data expanded to show the first 10 min in more detail. Each point represents the normalised relative fluorescence intensity of a minimum of 10 cells per experiment and the mean of 3 independent experiments ± SEM.

component of strand break repair (2 min) suggesting that NIR multiphoton laser microbeam irradiation may not induce these very simple damages or XRCC1 may not be required for the repair of this sub-set of damage. Following laser microbeam irradiation, the half-life of the component of repair involving XRCC1 is consistent with the 2nd half-life observed for strand break repair (Table 1). The slow component of repair involving XRCC1-YFP may represent the repair of complex DNA damage that is more difficult to repair than simple damage (Fig. 4) or alternatively may represent the repair of DNA DSBs by an back-up non-homologous end joining pathway that has been proposed to involve XRCC1 (Fig. 4). DSBs would have slower repair kinetics than the DNA lesions. The slow kinetics of XRCC1-YFP is similar to the slow component of strand break repair is shown by Dikomey and Franzke (~200 min, Table 1, (8)).

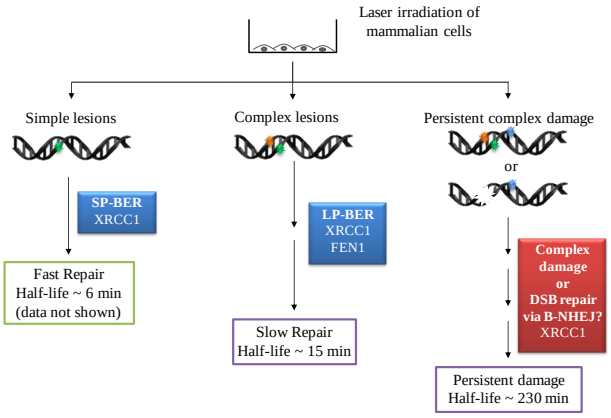

Figure 4: Schematic diagram illustrating the induction and repair of DNA damage following laser microbeam induced damage.

FEN1-GFP is recruited more slowly to induced DNA damage than XRCC1 (~5 min vs. ~2 min, respectively). The role of

FEN1 in LP-BER (Fig. 1) has been shown to be the predominant repair pathway for repair of complex DNA lesions including complex SSBs. Repair involving FEN1-GFP occurs with single exponential decay kinetics suggesting repair is by a single process consistent with the second component of DNA strand break repair (~15 min [Fig. 4 and Table 1 (8)]). The similarity of the loss of XRCC1-YFP and FEN1-GFP may indicate that XRCC1 is involved in LP-BER. The lack of significant slow process with FEN1-GFP would be consistent with the slow loss of XRCC1-YFP results for repair of DSBs or some other form of damage which does not require BER.

	1st Half-Life (% relative contribution)	2nd Half-Life (% relative contribution)	3rd Half-Life (% relative contribution)
DNA strand break repair (Dikomey & Franzke, 1986)	**2 min (70%)**	**17 min (25%)**	**200 min (5%)**
XRCC1-YFP		**NIR laser microbeam 15 min (70%)**	**NIR laser microbeam 230 min (30%)**
FEN1-GFP		**NIR laser microbeam 15 min**	

Table 1: Comparison of kinetic half-lives of BER proteins at induced DNA damage compared to those of DNA strand breaks (8).

Conclusions

It is concluded that sub-sets of NIR laser microbeam induced DNA damage are repaired by XRCC1 and FEN1. XRCC1 and FEN1 repair DNA damage with a half-life of ~15 min which may represent processing of complex damage by BER. XRCC1 although not FEN1 is involved in the repair of a subset of DNA damage with long repair kinetics (~230 min) which may represent very complex DNA damage of DNA or DSBs which are not repaired by BER.

Acknowledgements

We would like to thank CRUK and the MRC council for funding the studentship of S. Cooper.

References

1. Gulston, M., de Lara, C., Jenner, T., Davis, E., & O'Neill, P. (2004) Nucleic Acids Res 32, 1602-1609.

2. Lomax Cunniffe S, O'Neill P.Biochemistry. (2004) 43(34):11017-26

3. Robertson, A. B., Klungland, A., Rognes, T., & Leiros, I. (2009) Cell Mol Life Sci 66, 981-993.

4. Zharkov, D. (2008) Cell. Mol. Life Sci. 65 1544 – 1565

5. Caldecott, K. W. (2003) DNA Repair (Amst) 2, 955-969.

6. Harper, J. V., Reynolds, P., Leatherbarrow, E. L., Botchway, S. W., Parker, A. W., & O'Neill, P. (2008) Photochem Photobiol 84, 1506-1514.

7. Reynolds, P. (2009) PhD thesis. Reading University.

8. Dikomey, E. & Franzke, J. (1986) Radiat Environ Biophys 25, 189-194.